Int J Mech Mater Des
https://doi.org/10.1007/s10999-023-09683-4

A contact analysis for unconventional mounting processes of angular ball bearings

Simone Dreon · Lorenzo Scalera · Enrico Salvati

Received: 11 July 2023 / Accepted: 10 September 2023
© The Author(s) 2023

Abstract Rigorous protocols must be followed when mounting ball bearings to avoid structural damage and subsequent malfunctioning or unexpected failures. Unconventional mounting procedures may produce excessive contact pressures between the elements of the bearing, therefore the whole process must be well-understood and modelled to prevent unwanted effects. Specifically for angular ball bearings, fitting axial forces should always be applied over the raceway subjected to the shrink-fit to avoid contact forces arising on the ball. In the present study, such an axial force is applied unconventionally, such that the axial force is transferred to the shrink-fit raceway through the balls. In this scenario, the evaluation of the contact areas and the pressure distributions is accomplished by exploiting both analytical and FEM approaches, supported by bespoke experimental tests to determine the relevant frictional coefficients and mounting forces. The study demonstrated how analytical methods can successfully replace more demanding FEM-based tools for the evaluation of the bearing mounting force and contact pressure and extent. FEM modelling can, however, be more accurate when dealing with more generic boundary conditions and more intricate geometrical features involved.

S. Dreon · L. Scalera · E. Salvati (✉)
University of Udine, Udine, Italy
e-mail: enrico.salvati@uniud.it

Keywords Ball bearings · Contact · Shrink fit · Hertz theory · FEM

List of symbols

(r_x, r_y)	Principal curvatures
α^*	Nominal ball contact angle
α_0	Contact angle with the outer raceway
α_i	Contact angle with the inner raceway
δ	Coupling interference
μ_b	Coulomb's friction coefficient between ball and raceway
μ_h	Friction coefficient between the housing and the outer raceway
ν	Poisson's ratio
ρ	Radial coordinate of the bearing
σ_b	Tensile strength
σ_s	Yield strength
θ	Circumferential coordinate of the bearing
ζ	Axial coordinate of the bearing
A	First composite radius
a	Major axes of the elliptic contact area
B	Second composite radius
b	Minor axes of the elliptic contact area
E	Young's elastic modulus
e	Eccentricity of the contact area
$E(e)$	Elliptic integral of the second kind according to Hertz's theory
E^*	Composite elastic modulus
F_a	Shrink-fit force
F_s	Force exchanged between one ball and the raceway

Published online: 05 October 2023

$F_{a,0}$	Axial force at the outer raceway for the determination of the friction
$K(e)$	Elliptic integral of the first kind according to Hertz's theory
n	Number of balls
$p(x, y)$	Contact pressure distribution
p_0	Maximum pressure in the contact area
p_{int}	Interference fit pressure
Q	Approximated contact forces at the inner and outer raceways
Q_0	Ball/raceway contact force for the outer raceway
Q_i	Ball/raceway contact force for the inner raceway
Q_s	Contact force for each ball
R_0	Radial force component at the outer raceway
r_e	Nominal radius of the interface
r_h	Measured radius of the housing
R_i	Radial force component at the inner raceway
r_i	Nominal inner radius of the outer raceway
$r_{e,b}$	Measured external radius of the bearing
R_{int}	Interference force
T^*	Coulomb's frictional force at the interference between outer raceway and housing
T_0	Frictional force at the outer raceway
T_i	Frictional force at the inner raceway
u	Displacement
W	Bearing width
x	Contact area major axis
y	Contact area minor axis

1 Introduction

Rolling bearings are widely used mechanical elements that have remarkably contributed to the technological progress of humankind in the last centuries (Hamrock and Anderson 1983). Thanks to the industrial revolution, a relevant effort by the industrial and scientific community to advance the understanding of the working principles and structural aspects have made this element extremely efficient and reliable under a wide range of environmental and loading conditions. Although their relatively simple working principle, the interaction of the parts that constitute rolling bearings makes the structural analysis rather complex. The key parts are the outer and inner rings (races) and the rotating elements. Indeed, only the advent of advanced numerical calculation tools has allowed researchers to overcome the limitations of analytical solutions and therefore to take the accuracy of structural issues to a higher level (Demirhan and Kanber 2008; Singh et al. 2014; Xi et al. 2021).

Amongst all the types of rolling bearings, ball bearings are certainly the most popular. For this important family of bearings, several studies were carried out, and reported in the literature, dealing with the structural analysis in specific operational conditions through numerical methods, such as the finite element method (FEM). Examples are: contact stress analysis (Yongqi et al. 2012; Zhaoping and Jianping 2011; Lostado et al. 2016), stiffness (Guo and Parker 2012), fatigue analysis (Deng et al. 2013), crack propagation (Nazir et al. 2018), dynamics analysis (Holm-Hansen and Gao 2000) [also in the presence of material defects (He et al. 2022)], and corrosion (Schwack et al. 2018).

It is important to highlight that the structural integrity of rolling bearings is not exclusively influenced by the operational condition, but also by the mounting process. Indeed, frequently, such a mounting operation is accomplished by shrink fit which inevitably introduces additional stress on the races of the bearing and thus on the rolling parts. Not only the stress state obtained at the end of the fitting process is important, but it is vital to comprehend the whole process to make sure no unexpected permanent deformation or damage to the parts of the bearings occurs. As happens to other specific structural problems, this aspect can be studied either by analytical or numerical methods. For example, FEM can be successfully employed to simulate the shrink fits process including the effect of thermal expansion and additional stresses due to centrifugal forces on the preload (Kim et al. 2009). To make sure all the interactions between parts are correctly modelled, contact phenomena must be accurately captured. To do so, the Hertzian theory is a good candidate if an analytical approach is pursued and applicable (Anoopnath et al. 2018; Azianou et al. 2013; Shin and Hur 2022). Conversely, if the ratio of the rolling element over the most representative dimension of the races is high, then FEM should be used by employing contact element formulations. This is not the only limiting applicability condition of the Hertzian theory contact though, other aspects can only be captured by FEM simulations, such as the complex geometry of races, the presence of cages

(Fang et al. 2007), and lubrication conditions (Lovell and Khonsari 1999).

The fitting process implies axial forces to be applied over the side flat faces of the races. Particularly for angular contact ball bearings, only one race of the bearing can be subjected to such an axial force, therefore the internal clearance between the races and the balls vanishes with a consequent arising of high contact pressure (Schwack et al. 2018; Liu et al. 2019). In particular, a relatively recent study highlighted that the stresses arising from the assembling process have a noteworthy influence on the bearing dynamic properties and stiffness, in case the mounting axial force is applied at the inner race (Zhang et al. 2017). Structural aspects of this specific class of ball bearings were carried out in the last years, mainly focusing on contact stresses due to externally applied loads (Turek et al. 2019; Deng et al. 2017), global stiffness and damping (Hagiu and Gafitanu 1997), and in the context of nonlinear dynamic models of rotor systems (Wang et al. 2017). Nevertheless, to the best of the authors' knowledge, no studies have been comprehensively done yet on the stresses arising during the fitting process and their effects on the structural properties of the bearing.

This paper aims at evaluating the contact stresses arising while mounting an angular contact ball bearing by axially pressing its inner raceway, while the interference fit occurs at the outer raceway. The approach pursued herein relies on a twofold mathematical study, i.e., Hertzian contact theory and FEM modelling. An extensive experimental investigation is conducted to assess the friction coefficients involved in a case study and a dedicated experiment was aimed at evaluating the actual force required to accomplish the shrink fit. The accuracy of the two proposed methods is quantitatively assessed and extensively discussed, alongside the practical implications of the findings.

2 Problem statement

This section reports all the relevant details to frame the problem. All the components involved and the way these are coupled are described, while outlining the issues that may arise during this procedure that are addressed in the present study. Geometrical and material details are provided in "Appendix 1.1" for the in-depth analysis of the problem.

The specific analysed problem refers to the assembly depicted in Fig. 1a. As illustrated in the exploded-view drawing in Fig. 1b, the system consists of four parts labelled from (1) to (4); noting that parts (1) and (2) are the same. The engineering design solutions shown in the figure enable a shaft to freely rotate in a stationary case (housing) labelled as (3). Given that the shaft may experience axial forces due to external loads in both directions, a pair of angular contact ball bearings (1) and (2) is chosen to avoid unwanted axial movements of the shaft. The seeger (4) is mounted in the housing (3) to facilitate the positioning of the bearings during mounting and avoid their axial movement in one direction.

According to Fig. 1b, the mounting sequence is the following: (i) the bearing (1) is inserted in the housing (3) by axially pushing it from the left-hand side of the case; (ii) the seeger is inserted from the left-hand side; (iii) the second bearing (2) is inserted in the same way as done for the bearing (1) until locked by the contact with the seeger side. The insertion process requires a sufficiently high axial force to overcome the tangential force due to the friction between the two sliding surfaces and the relative change of the two coupled components' diameters due to the shrink fit. For this reason, the mounting axial force can be applied exclusively over the outer race to avoid excessive loading on the inner race and therefore to limit the load experienced by the balls of the bearings. At this stage, the shaft can be mounted, together with all the other ancillary parts.

To perfect the assembly of the system, the final mounting step must ensure that the bearing (1) correctly sits against the seeger. Unfortunately, due to the specific geometrical configuration of the housing (3) on its right-hand side, bearing (1) cannot be pushed against the seeger by pressing the outer race, at least by using conventional tools. For this reason, the only way to rapidly accomplish this task is the application of an axial load over the inner race from the right-hand side, as displayed by the arrows in Fig. 2. Such a mounting solution does not ensure that the structural integrity and functionality of the bearing are not compromised by the mounting itself. Indeed, excessive contact pressures may arise between the balls and the two races, which may potentially lead to harmful plastic deformations. Therefore, a detailed analysis is

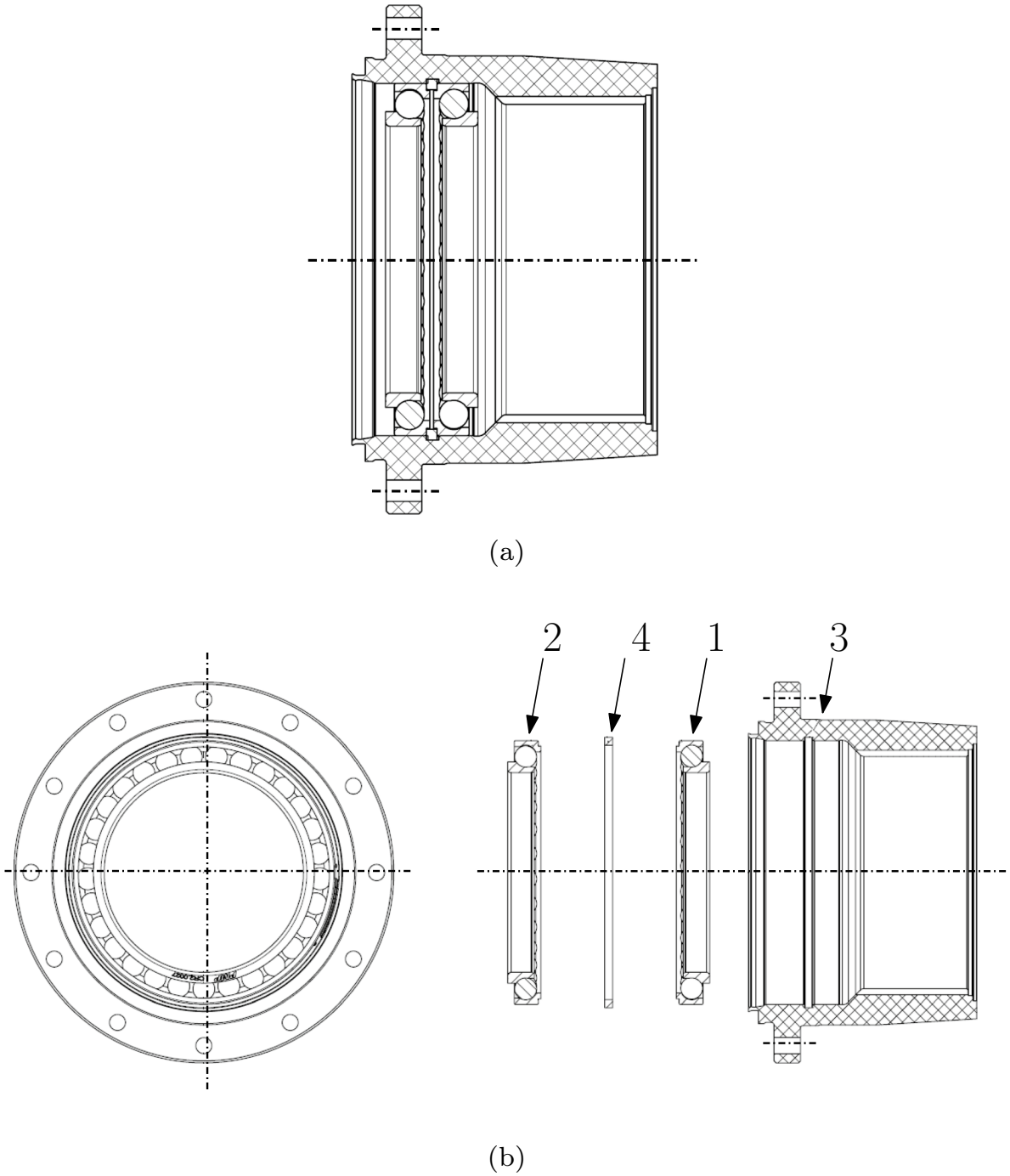

Fig. 1 Final configuration of components (**a**); frontal view and exploded view (**b**)

fundamental to assess whether the proposed assembling procedure routinely is acceptable.

In this paper, two different methods are proposed to determine the maximum pressure that arises between the balls and the bearing races, induced by this specific unusual installation protocol. Subsequently, the evaluated pressure contact is employed

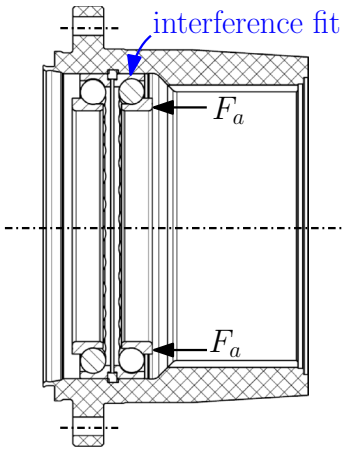

Fig. 2 Final stage of the bearing fitting by pressing on the inner ring

to assess whether the mounting operation can be safely performed.

3 Experimental methods

Experimental tests were conducted to determine the unknowns of the problem and corroborate the numerical calculations. Two sets of experimental tests were carried out to:

(i) Evaluate the housing friction coefficient μ_h through the application of an axial force at the outer raceway;
(ii) Evaluate the shrink fit force F_a when the bearing is axially loaded at the inner raceway.

Regarding (i), two experimental tests are performed to obtain an estimate of the Coulomb's friction μ_h between the housing and the outer raceway of the bearing, a pivotal coefficient in quasi-static and dynamics problems (Marino and Cicirello 2020). In order to achieve so, a hydraulic press is employed to accomplish the shrink fit through the application of a force, as displayed in Fig. 3; by controlling the displacement. According to the image, a linear actuator is coupled with a bearing mounting fixture that fits the hosting case, which accommodates the ball bearing, and it ensures that the force is evenly distributed over the outer raceway of the bearing. The tests were performed in absence of lubrication. During the test,

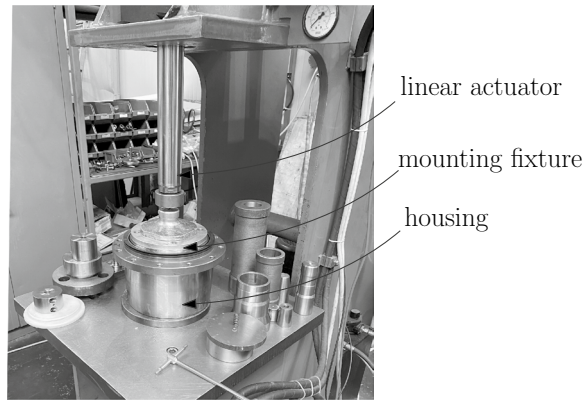

Fig. 3 Experimental setup. (Color figure online)

both displacement and applied force were recorded through a data acquisition unit. In this way, the force required to slide the bearing was recorded for further calculations and assessment of the friction coefficient μ_h. The experimental test to determine the shrink fit force (ii) was carried out by axially pressing the inner raceway of a bearing in displacement control mode, using a bespoke mounting fixture, employing an analogous setup as shown in Fig. 3. One test was conducted for this purpose.

Additional experimental activities were conducted to precisely characterise the involved geometries. As it will be shown later, it is of utmost importance to precisely measure the diameters of the fitted elements in order to evaluate the interference (δ) and therefore the interference force (R_{int}) arising when the two elements are coupled; which will be shown later in detail. To accomplish this task, a Zeiss PRISMO coordinate measuring machine (CMM) was used.

4 Analytical calculations

Theoretical analytical formulations are employed in this study to quantitatively estimate the effect of the fitting process on the contact between balls and races. With this objective, the fitting force must be evaluated first to appreciate the force applied to the balls at the contact with the raceways. This task is accomplished by invoking thick-walled cylinders' formulations and accounting for friction. Subsequently, Hertz's contact theory is recalled in evaluating the contact pressure distribution.

4.1 Bearing fitting force and ball/raceways contact force

To analytically evaluate the minimum force required to accomplish the fitting of the bearing F_a, and therefore the contacts ball/raceways forces, it is necessary to analyse the relevant components of forces involved that the parts of the ball bearing exchange with each other; similarly to the approach followed by Jedrzejewski and Kwasny (2010). To help the reader comprehend the problem, a schematic illustration is presented in Fig. 4a. It is important to highlight that the ball contact angle may vary from the nominal value α^* when in service and, on top of that, the contact angle with the outer raceway α_0 may differ from the contact angle with the inner raceway α_i.

First of all, the ball/raceways contact forces are named as Q_i and Q_0, respectively for the inner and outer raceways. At the inner raceways, the contact force Q_i gives rise to a frictional force:

$$T_i = \mu_b \, Q_i \tag{1}$$

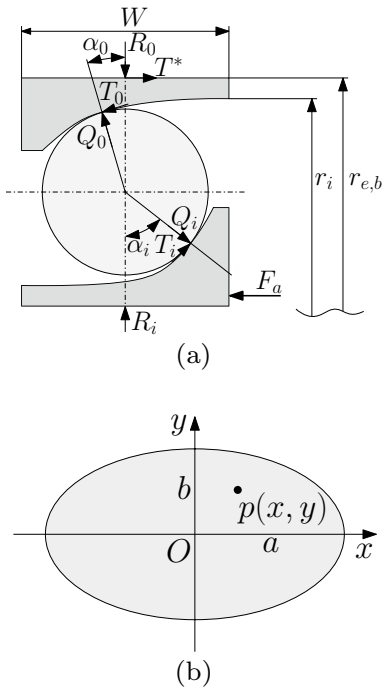

Fig. 4 **a** Force contributions diagram and characteristic dimensions; **b** elliptic contact area reference diagram

where μ_b is the Coulomb's friction coefficient between the ball and the raceway. The choice of such a Coulomb's friction formulation is justified by the quasi-static nature of the mounting process, which does not lead to relevant rolling; that would occur if the bearing was in service. Both the axial and radial contributions of T_i and Q_i must be balanced to achieve force equilibrium. As far as the radial components at the inner raceway are concerned, their sum will be:

$$R_i = Q_i \cos \alpha_i - T_i \sin \alpha_i \tag{2}$$

Given that during the fitting procedure the shaft is not present, the only radial component of the force that can exist is due to the presence of the hoop stress. It is worth commenting that the presence of a hoop stress and a gradient of radial stress in the inner raceway inevitably generates a radial displacement—this effect is neglected in the presented analytical evaluation. Concerning the axial equilibrium of the inner raceway, the equilibrium conditions are met when an external axial force is applied, which is exactly the fitting force F_a, that is:

$$F_a = Q_i \sin \alpha_i - T_i \cos \alpha_i \tag{3}$$

To estimate the contact force at the inner raceway, it is necessary to know the value of the axial fitting force. To do so, the equilibrium of forces at the outer raceway is required. At the outer raceway, the contact force between the balls and the raceway can be evaluated by considering the radial equilibrium of the balls that leads to:

$$Q_0 = Q_i \left(\frac{\mu_b \sin \alpha_i - \cos \alpha_0}{\mu_b \sin \alpha_0 - \cos \alpha_i} \right) \tag{4}$$

At this point, the equilibrium at the outer raceway can provide the remaining information to fully estimate the required axial fitting force. Firstly, the radial equilibrium of force is met when an external force (housing radial force) is present:

$$R_0 = Q_0 \cos \alpha_0 - T_0 \sin \alpha_0 + R_{int} \tag{5}$$

where T_0 is the frictional force at the outer raceway defined as: $T_0 = \mu_b \, Q_0$, whereas R_{int} is the interference shrink fit force that refers to the contribution of the pressure arising at the interface due to the interference. Thus, upon knowledge of the interference fit p_{int}, R_{int} can be assessed as:

$$R_{int} = p_{int}\, 2\pi r_e W \tag{6}$$

where r_e and W are the nominal radius of the interface and the bearing width, respectively, as displayed in Fig. 4a. The interference pressure p_{int} can be promptly evaluated through the analytical formulation provided by the thick-walled cylinders theory, when the coupling interference is known. The closed form of such a pressure is:

$$p_{int} = \frac{E\delta}{r_e}\left(\frac{r_e^2 - r_i^2}{\left(r_e^2 + r_i^2\right) - \nu\left(r_e^2 - r_i^2\right)}\right) \tag{7}$$

where r_i is the nominal inner radius of the outer bearing raceway, as displayed in Fig. 4a. While E and ν are the elastic properties of the material, as reported in Table 1. The coupling interference δ is the difference between the two coupled radii involved, defined as:

$$\delta = |r_{e,b} - r_h| \tag{8}$$

where $r_{e,b}$ is the real external radius of the bearing and r_h is the actual radius of the housing.

To achieve sliding of the bearing while mounting, a limit state analysis can be performed by considering the axial contributions of forces at outer raceway:

$$Q_0 \sin\alpha_0 + T_0 \cos\alpha_0 > T^* \tag{9}$$

where T^* is the Coulomb's frictional force developed at the interface between the outer raceway and the housing, that is:

$$T^* = \mu_h R_0 \tag{10}$$

where μ_h is the coefficient of static friction between the housing and the outer raceway.

By substituting the forces T_0 and T^* in Eq. (9), it is possible to explicitly show the contact pressure at the outer raceway:

Table 1 100Cr6—AISI 52100 material properties

Property	Unit	Value
Poisson's ratio (28 ÷ 125°)	(–)	$\nu = 0.29$
Elastic modulus	(GPa)	$E = 207$
Tensile strength	(MPa)	$\sigma_b = 2157$–2550
Yield strength	(MPa)	$\sigma_s = 1667$–1814
Hardness	(HRC)	61–65

$$Q_0 > \frac{2\pi WE\delta\mu_h}{\sin\alpha_0 - \mu_h\cos\alpha_0 + \mu_h\mu_b\sin\alpha_0 + \mu_b\cos\alpha_0}\left(\frac{r_e^2 - r_i^2}{\left(r_e^2 + r_i^2\right) - \nu\left(r_e^2 - r_i^2\right)}\right) \tag{11}$$

Details of this derivation are shown in "Appendix 1.2".

Similarly, it is possible to express the contact pressure ball/raceway at the inner raceway by invoking Eq. (4):

$$Q_i > \frac{2\pi WE\delta\mu_h(\mu_b\sin\alpha_0 - \cos\alpha_i)}{(\mu_b\sin\alpha_i - \cos\alpha_0)(\sin\alpha_0 - \mu_h\cos\alpha_0 + \mu_h\mu_b\sin\alpha_0 + \mu_b\cos\alpha_0)}\left(\frac{r_e^2 - r_i^2}{\left(r_e^2 + r_i^2\right) - \nu\left(r_e^2 - r_i^2\right)}\right) \tag{12}$$

The obtained formulae can be simplified if the friction coefficient at the contact between the balls and the raceways is very low, i.e., $\mu_b << \mu_h$. Therefore, Eq. (11) becomes:

$$Q_0 > \frac{2\pi WE\delta\mu_h}{\sin\alpha_0 - \mu_h\cos\alpha_0}\left(\frac{r_e^2 - r_i^2}{\left(r_e^2 + r_i^2\right) - \nu\left(r_e^2 - r_i^2\right)}\right) \tag{13}$$

thus the contact force at the inner raceway:

$$Q_i > \frac{2\pi WE\delta\mu_h\cos\alpha_i}{\cos\alpha_0(\sin\alpha_0 - \mu_h\cos\alpha_0)}\left(\frac{r_e^2 - r_i^2}{\left(r_e^2 + r_i^2\right) - \nu\left(r_e^2 - r_i^2\right)}\right) \tag{14}$$

For the sake of brevity, the derivation steps are omitted here. The reader can refer to "Appendix 1.2" for further details.

Besides the measurements of the geometrical dimensions and material properties, it is evident that a precise evaluation of the contact forces requires an appropriate assessment of the contact angles and friction coefficients. It is important to make some important observations regarding the former at this stage. As reported by Liao et al., the contact angles (α_i and α_0) are highly affected by the bearing angular velocity but, in most of the practical cases, either when the externally applied axial force is sufficiently high or the angular velocity is low (less than 3000 rpm), the sum of the contact angle mismatches, from the nominal value, is equal to twice the nominal contact angle (Jedrzejewski and Kwasny 2010; Liao and Lin 2002):

$$2\alpha^* = \alpha_0 + \alpha_i \tag{15}$$

Importantly, according to the results shown by Liao and Lin (2002), when the angular velocity is very low and the axial force is high, the two contact angles tend to assume the same value and converge to the nominal value. Given that in the present study the velocity is null, and the axial force is supposed to be high, it is possible to hypothesise that $\alpha_0 = \alpha_i = \alpha^*$. As a consequence, this approximation is made and the contact forces, both at the inner and outer raceways, can be retrieved as:

$$Q > \frac{2\pi WE\delta\mu_h}{\sin\alpha^* - \mu_h\cos\alpha^*}\left(\frac{r_e^2 - r_i^2}{\left(r_e^2 + r_i^2\right) - \nu\left(r_e^2 - r_i^2\right)}\right) \tag{16}$$

4.2 Contact pressure evaluation

Once evaluated the total force exchanged between the raceways and the balls Q, it is possible to evaluate the contact pressure distribution at each contact point ball/race through Hertz's theory. First of all, the problem can be locally studied by partitioning the full domain and by exploiting the cyclic symmetry of the problem. In general, ball bearings consist of a number n of balls, therefore, according to Fig. 4b, the force exchanged between only one ball and the raceways can be assessed as:

$$F_s = \frac{F_a}{n} \tag{17}$$

Similarly, the total contact force Q can be partitioned into n points of contacts, therefore, the contact force for each ball is:

$$Q_s = \frac{Q}{n} \tag{18}$$

The present contact problem falls within the category of ellipsoidal bodies, at least this is true locally. In this scenario, two principal curvatures can be defined locally for each surface (or body), i.e., ($r_{x,1}$, $r_{y,1}$) for the body labelled as 1, and ($r_{x,2}$, $r_{y,2}$) for the second body, 2. According to Hertz's theory, two composite radii A and B can be found as:

$$\begin{aligned} 2A &= \frac{1}{r_{x,1}} + \frac{1}{r_{x,2}} \\ 2B &= \frac{1}{r_{y,1}} + \frac{1}{r_{y,2}} \end{aligned} \tag{19}$$

According to Hertz' theory, the pressure distribution over the contact area of two interacting surfaces assumes an elliptic shape and can be fully defined by using a Cartesian coordinate system (x, y), according with Fig. 4b, as follows:

$$p(x,y) = p_0\sqrt{1 - \frac{x^2}{a^2} - \frac{y^2}{b^2}} \tag{20}$$

where p_0 is the maximum pressure in the contact area. While a and b are the major and minor axes determining the extent of the contact area and they can be found respectively as:

$$\begin{aligned} a &= \left(\frac{3Q_s[K(e) - E(e)]}{2\pi e^2 E^* A}\right)^{1/3} \\ b &= a\sqrt{1 - e^2} \end{aligned} \tag{21}$$

In which E^* is the composite modulus of elasticity, defined through the following expression by knowing the elastic propertied of the two materials involved in the contact:

$$\frac{1}{E^*} = \frac{1 - \nu_1^2}{E_1} + \frac{1 - \nu_2^2}{E_2} \tag{22}$$

while $K(e)$ and $E(e)$ are complete elliptic integrals, of the first and second kind respectively, and e is the eccentricity of the Hertzian contact. The solution of these three terms can be iteratively calculated from the following system of equations, given that the composite curvature radii are known:

$$\begin{aligned} K(e) &= \int_0^{\pi/2} \frac{d\vartheta}{\sqrt{1 - e^2\cos^2\vartheta}} \\ E(e) &= \int_0^{\pi/2} \sqrt{1 - e^2\cos^2\vartheta}\, d\vartheta \\ \frac{B}{A} &= \frac{1}{[K(e) - E(e)]}\left[\frac{E(e)}{1 - e^2} - K(e)\right] \end{aligned} \tag{23}$$

More details about the determination of these quantities and their physical significance can be found elsewhere (Barber 2018). In any case, a good approximation of the eccentricity is found as:

$$e = 2\sqrt{\left(\frac{1}{3} - \frac{A}{3B}\right)} \tag{24}$$

By integrating the pressure distribution seen in Eq. (20) over the contact area it is possible to evaluate the contact force:

$$\begin{aligned} Q_s &= 4\int_0^a \int_0^{b\sqrt{1-x^2/a^2}} p_0 \sqrt{1 - \frac{x^2}{a^2} - \frac{y^2}{b^2}}\, dxdy \\ &= \frac{2\pi abp_0}{3} \end{aligned} \tag{25}$$

Therefore, the maximum pressure in the contact area is:

$$p_0 = \frac{3Q_s}{2\pi ab} \tag{26}$$

5 Finite element modelling analysis

In this section, numerical simulations are set up and performed to corroborate the results obtained through the analytical calculations. In this study, ANSYS Workbench 2022 R1 software was employed to discretise, apply boundary conditions and solve the FEM simulation.

Given the geometrical nature of the three-dimensional assembly that is sought to study, i.e., cyclic symmetry, it is possible to considerably reduce the computational effort by modelling only one azimuthal sector containing one ball. As displayed in Fig. 5a, only a sector of the whole geometry is extracted and modelled (in red). Following, the extracted model was subdivided into several sub-domains with the aim of facilitating the realization of a structured mesh, particularly at the contact regions, as shown in Fig. 5b. For example, the considered sphere of the model was divided into 186 domains. SOLID186 and SOLID187 elements were utilized to discretise the analysed structure; both having quadratic shape functions in a Lagrangian formulation. In particular 20-node SOLID186 elements were employed to model regions of interest, while the 10-node element SOLID187 was primarily employed do discretise regions away from the focus of the study, i.e., where structured mesh was not necessary. It is important to point out that a mesh convergence test was carried out by refining the mesh at the contact area and surrounding regions. As a result of the mesh convergence test, the minimum dimension of the mesh elements turned out to be equal to 0.05 mm in the contact area, whereas the surfaces of the domains adjacent to the contact were discretised with elements of 0.5 mm in size. A linear elastic isotropic material constitutive law was chosen and the material parameters are reported in Table 1.

According to Fig. 6, the displacement boundary conditions are applied such that the cylindrical symmetry is enforced; radial ρ and circumferential ϑ displacements are intrinsically constrained. Concerning the constraints on the sphere, it must be ensured that it is free to translate in both ρ and ζ directions due to the tolerance allowed by the geometry of the component. As a result, the only constraint to be imposed on the rolling element is in the circumferential direction ϑ, which is required to compensate for the absence of the cage in the model geometry (this condition was applied away from the contact regions, i.e., at the centre of the spherical

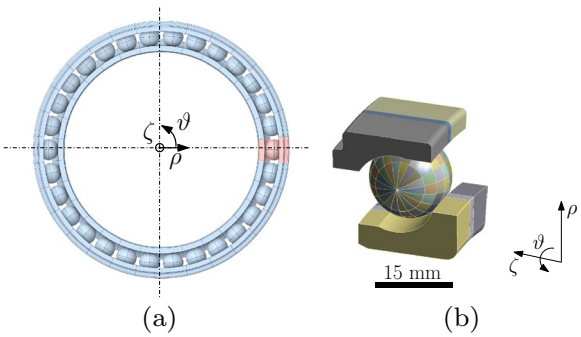

Fig. 5 3D model of the ball bearing. **a** Overview; **b** sector domain

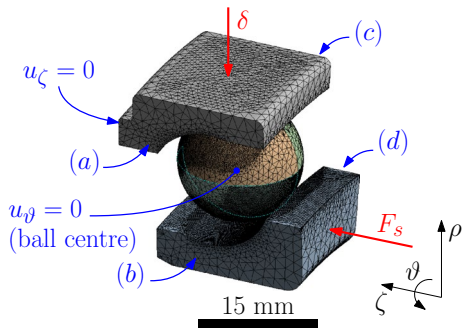

Fig. 6 Applied boundary conditions schematisation. Cyclic symmetry is applied to faces (**a**–**d**)

element). The axial force F_s was applied at the inner race. The interference fit was modelled by imposing a negative displacement δ along the radial direction ρ over the surface that goes into contact with the housing. Eventually, the outer race was constrained, as shown in Fig. 6, such that no translation in the ζ direction was allowed; this condition allowed for a faster computation, keeping the same accuracy in the evaluation of the contact forces, as compared with the conditions in which friction is present at the interface race/housing.

To model the contact between the sphere and the tracks, rolling friction is considered equal to 0.002. In this regard, it is important to highlight that, given the small size of the coefficient itself, this could be neglected by using a frictionless formulation; this aspect has been already unshadowed in Eq. (12). Nevertheless, in order to mitigate the risk of numerical convergence issues, it was decided to incorporate such a minor frictional behaviour in the model. Sensitivity tests were performed to prove the correctness of this assumption.

The contact problem is solved according to the Augmented Lagrange formulation. Since the Augmented Lagrange form is a penalty-based method, in which the normal stiffness factor was assumed to be 0.8, this choice did not produce excessive sliding issues and optimised the computational convergence. A parametric analysis was performed to select the most appropriate stiffness factor coefficient. This process started by assuming a very small value 0.05 to limit convergence issues. Then the value was increased to reduce the penetration depth while assuring the convergence of the simulation. The large sliding formulation was also activated.

6 Results and discussion

6.1 Experimental results

6.1.1 Housing/outer raceway friction coefficient

The application of an axial displacement at the outer raceway allowed for the estimation of the friction coefficient by monitoring the evolution of the axial force. The force required to accomplish the bearing mounting was monitored and recorded, two test results are shown in Fig. 7.

Due to the absence of lubricant, it is not straightforward to determine the friction coefficient unequivocally. Indeed, above a certain displacement, the force is subjected to relevant fluctuations and instabilities, as seen in Fig. 7. For this reason, a representative friction coefficient was evaluated by averaging the applied force from when the first sudden force increase occurs after the initial sliding (at around 3 s after the start of the test). By averaging the fitting force, the friction coefficient was assessed as follows:

$$\mu_h = \frac{F_{a,0}}{R_{int}} \tag{27}$$

where $F_{a,0}$ is the applied axial force at the outer raceway and R_{int} is the interference radial force. The latter can be evaluated for each specific test by recalling Eq. (6), and by measuring the actual dimensions of the external radius of the bearing outer raceway and the housing diameter. By averaging also the resulting friction coefficients from the two executed tests, the representative final value turned out to be 0.173. As compared with the rolling frictional coefficient of the ball/raceway contact, such a value is around two

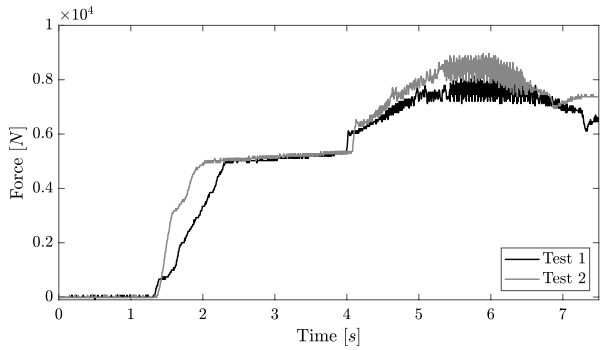

Fig. 7 Shrink fit axial force evolution when applied at the outer raceway

orders of magnitudes higher, so it justifies the simplification introduced in Eq. (13).

6.1.2 *Shrink fit force by pressing at the inner raceway, experiment versus theory*

The results of this test is highly affected by the precise evaluation of the radial interference occurring when mating the housing and the bearing. For the specific configuration employed in this study, a precise experimental measurements of the geometrical dimensions of the two analysed objects led to the conclusion that such a mismatch was $\delta = 31\,\mu$m. This information is fundamental for both the analytical and FEM calculations to properly account for the interference forces. Following, the application of an axial displacement through the linear actuator at the inner raceway produced the profile displayed in Fig. 8. The averaged force required to accomplish the mounting in this configuration turned out to be $F_a = 11797$ N. As far as the theoretical approach outlined in this study is concerned, the ball/raceways contact force was firstly assessed through Eq. (16). Subsequently, Eq. (3) was invoked to retrieve the axial fitting force applied, by neglecting the frictional forces. The outcome of such a calculation resulted in an axial force required to accomplish the fitting of $F_a = 13941$ N. Therefore, the agreement between the analytical and the experimental evaluations is satisfactory as the mismatch is of around 15%. A summary of all these outcomes is shown in Fig. 8. Additionally, it is worth noting that the experimental profile shows a relatively high degree of scatter, and some peaks of force approach very closely to the theoretically assessed value. A close-up diagram displayed in the inset of Fig. 8 reports a non-uniform jerking relative motion (i.e., stick–slip phenomenon) as the mounting progresses. In particular, higher stick–slip frequencies are observed at the initial stages, followed by an amplitude attenuation that makes difficult the assessment of the frequency and a third stage in which higher amplitude and low frequencies are observed.

6.2 Numerical results

6.2.1 *Ball/raceway contact pressure evaluation and comparison*

In this section the results concerning the analytical and numerical evaluation of contact pressure distributions, between the ball and the raceways, are shown. Because of the most critical contact region lies at the interface between the inner raceway and the ball, only the pressure arising in such a location was analysed. First of all, given that the experimentally evaluated axial fitting force is supposed to be more realistic, its fraction that is actually exerted over the cyclic domain, consisting on one single ball, was evaluated and turned out to be $F_s = 393$ N. The considered interference fit was the same as used before: $\delta = 31\,\mu$ m. For the sake of comparing the results obtained through the numerical (FEM) and the analytical (Hertz's) approaches, the 1-D pressure distribution profiles along the major and the minor axes of the contact ellipse are shown in Fig. 9a and b; the FEM contact pressure profile was projected over a reference curvilinear coordinate system to obtain a consistent reference with the analytical solutions according to the system of coordinated shown in Fig. 4b. Additionally, a contour plot of the pressure distribution is displayed in Fig. 9c, alongside a magnified image, over the inner raceway. The agreement between the theory and the FEM methods is more than satisfactory. Only very minor deviations

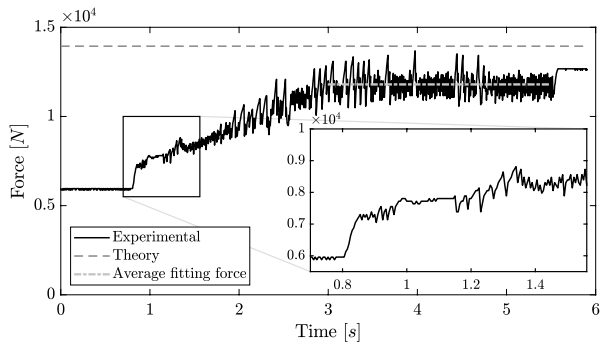

Fig. 8 Shrink fit force evolution when pressing at the inner raceway

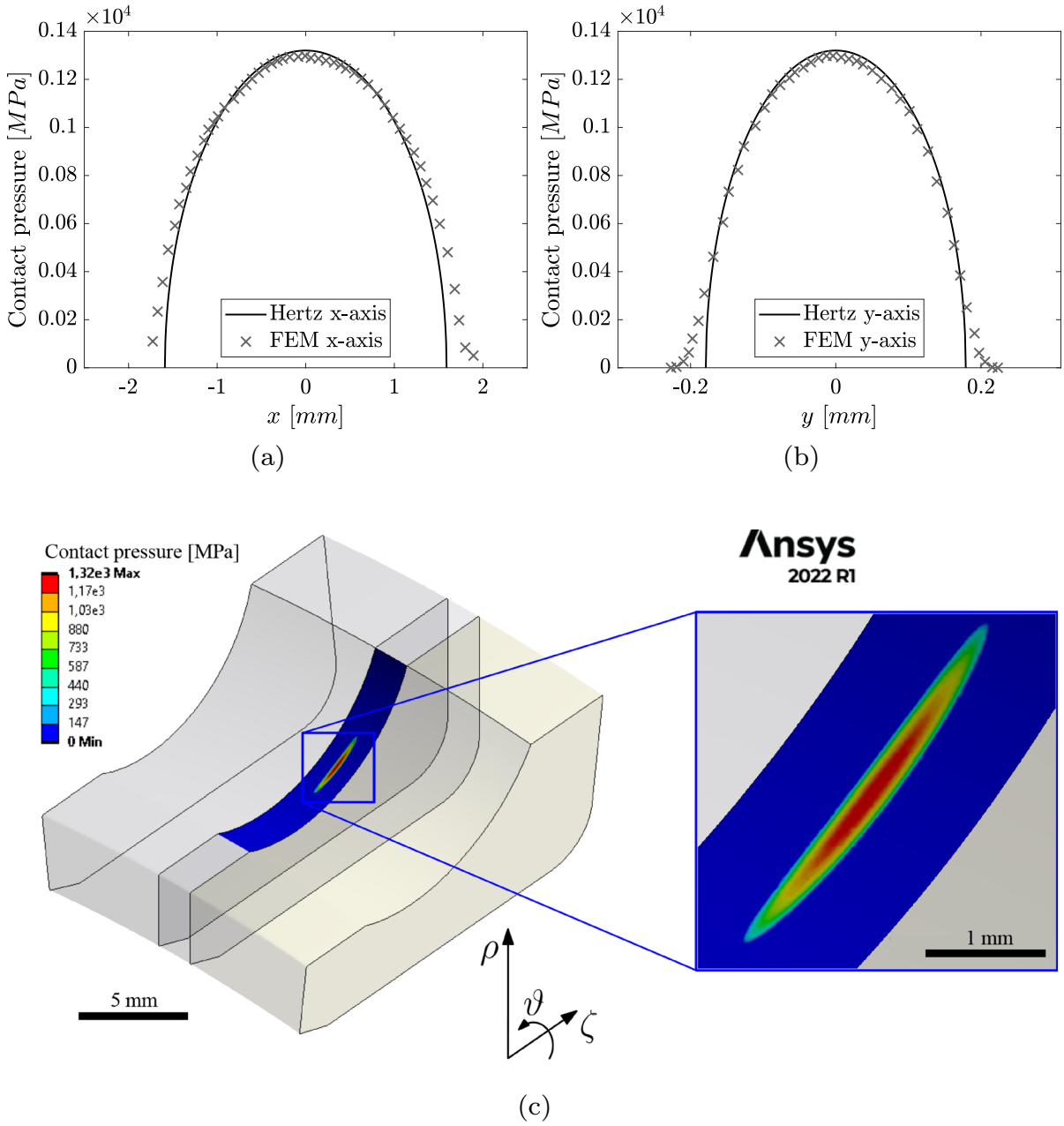

Fig. 9 Contact pressure distribution comparison between the inner raceway and the ball: analytical versus FEM. **a** and **b** distribution along the major and minor axes, respectively. **c** FEM contour plot and magnification of the contact area

can be observed at the periphery of the contact area where the FEM solution is actually capable of capturing also fine non-linear details. In spite of the contact angle of the rolling elements that may be slightly altered from the nominal value of 30°, the analytical solution provided a high degree of accuracy. The bearing manufacturer specifies that the bearing raceways allow a change of this angle between 25° and 32° during the service conditions (Shin and Hur 2022). Nevertheless, these extreme values are hardly reachable as the analysis conducted herein refers to a quasi-static scenario, as previously discussed in the

theoretical approach section. Overall, the analytical calculation can certainly be a less expensive route for the assessment of contact pressures generated during the shrink-fit process.

7 Conclusions

The present study proposed two approaches to assess the contact pressures arising when mounting angular ball bearings following an advised against route. The strengths and the limitations of the analytical approach, based on the thick-walled cylinders and the Hertzian contacts, to evaluate the required fitting force and the associated contact pressure between the raceways, balls and housing, were widely analysed and critically discussed. The key outcomes of the study can be summarized as follows:

- The friction coefficient at the sliding interface can be effectively evaluated experimentally by precise measurements of the interfering diameters, followed by a force-monitored mounting experimental test.
- The theoretical formulation can be a highly effective route to determine the interference pressure between the outer raceway and the housing. Thereby, the required axial shrink-fit force applied solely at the outer raceway can be effectively evaluated upon knowledge of the friction coefficient; this represents the conventional mounting route.
- The proposed analytical framework for the evaluation of the axial fitting force required to attain a shrink-fit of the bearing by pressing at the inner raceway may slightly overestimate the actual require force. The analysed case-study showed a mismatch of around 15%. This minor discrepancy is imputed to the geometrical approximation introduced when calculating the interference force through the thick-walled pressure vessels theory. FEM tools might be preferred when dealing with high magnitudes of interference fits.
- Hertz's contact theory resulted to be highly accurate to estimate both the contact extent and the contact pressure distribution.

Overall, the calculation methodology will enable engineers to determine whether the mounting process can be safely executed, i.e., without inducing any structural damage. Moreover, given its flexibility, it is possible to tune the boundary conditions (e.g., lubrication, interference) such that the structural integrity and functionality of the bearings are not impaired.

Funding Open access funding provided by Università degli Studi di Udine within the CRUI-CARE Agreement.

Data availability The datasets generated during and/or analysed during the current study are available from the corresponding author on reasonable request

Appendix 1

Appendix 1.1: Ball bearing details and materials

Two angular contact ball bearings are considered, which can bear a combination of axial and radial loads. The nominal dimensions and geometry of the ball bearing are displayed in Fig. 10, along with the characteristic nominal contact angle. Such a contact angle is defined as the imaginary line connecting the centers of the spheres and the inner race/sphere contact point, forming a 30° angle with respect to the radial direction. The considered ball bearing includes 30 balls, each one with a nominal diameter of 15.875 mm. The rings and rolling elements are made of 100Cr6—AISI 52100 bearing steel; whose mechanical properties are listed in Table 1. A Polyamide PA66 nylon, with an addition of 15% of glass fiber, is used for the cage.

It is important to highlight that the housing (42CrMo4 steel) presented relatively high characteristic thicknesses, which led to the assumption that its overall stiffness is much higher than the ball bearing radial stiffness, which was assumed as non-deformable.

Appendix 1.2: Contact force derivation

The derivation of the contact force is reported in the following.

$$Q_0 > \frac{T^* - T_0 \cos \alpha_0}{\sin \alpha_0} = \frac{T^*}{\sin \alpha_0} - T_0 \operatorname{cotan} \alpha_0 \qquad (28)$$

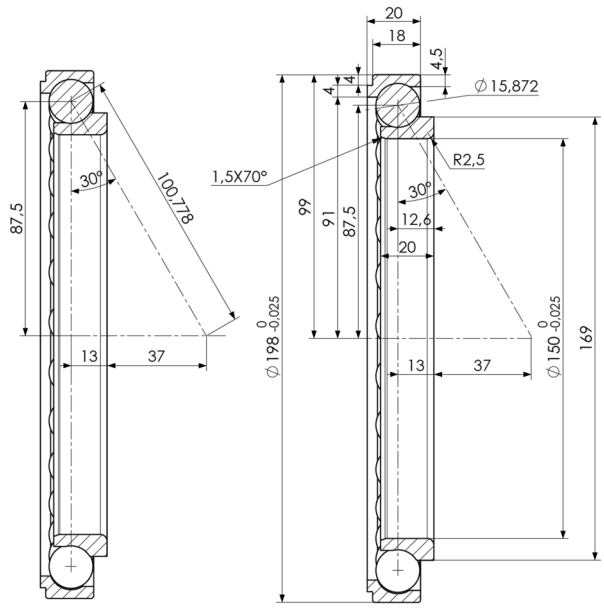

Fig. 10 Characteristic dimensions of the studied ball bearing. Dimensions are in millimiters

$$
\begin{aligned}
&> \frac{\mu_h}{\sin\alpha_0}\left[Q_0\cos\alpha_0 - T_0\sin\alpha_0 + R_{int}\right] - T_0\operatorname{cotan}\alpha_0 \\
&> \frac{\mu_h}{\sin\alpha_0}Q_0\cos\alpha_0 - \frac{\mu_h}{\sin\alpha_0}T_0\sin\alpha_0 \\
&\quad + \frac{\mu_h}{\sin\alpha_0}R_{int} - T_0\operatorname{cotan}\alpha_0 \\
&> \mu_h Q_0\operatorname{cotan}\alpha_0 - \mu_h\mu_b Q_0 + \frac{\mu_h}{\sin\alpha_0}R_{int} - \mu_b Q_0\operatorname{cotan}\alpha_0 \\
Q_0&\left[1 - \mu_h\operatorname{cotan}\alpha_0 + \mu_h\mu_b + \mu_b\operatorname{cotan}\alpha_0\right] > \frac{\mu_h}{\sin\alpha_0}R_{int} \\
Q_0 &> \frac{\mu_h R_{int}}{\sin\alpha_0 - \mu_h\cos\alpha_0 + \mu_h\mu_b\sin\alpha_0 + \mu_b\cos\alpha_0}
\end{aligned}
\tag{29}
$$

In case μ_b assumes low values the following is obtained:

$$
Q_0 > \frac{\mu_h R_{int}}{\sin\alpha_0 - \mu_h\cos\alpha_0} \tag{30}
$$

Open Access This article is licensed under a Creative Commons Attribution 4.0 International License, which permits use, sharing, adaptation, distribution and reproduction in any medium or format, as long as you give appropriate credit to the original author(s) and the source, provide a link to the Creative Commons licence, and indicate if changes were made. The images or other third party material in this article are included in the article's Creative Commons licence, unless indicated otherwise in a credit line to the material. If material is not included in the article's Creative Commons licence and your intended use is not permitted by statutory regulation or exceeds the permitted use, you will need to obtain permission directly from the copyright holder. To view a copy of this licence, visit http://creativecommons.org/licenses/by/4.0/.

References

Anoopnath, P., Babu, V.S., Vishwanath, A.: Hertz contact stress of deep groove ball bearing. Mater. Today Proc. **5**(2), 3283–3288 (2018)

Azianou, A.E., Debray, K., Bolaers, F., Chiozzi, P., Palleschi, F., et al.: Modeling of the behavior of a deep groove ball bearing in its housing. J. Appl. Math. Phys. **1**(4), 45–50 (2013)

Barber, J.R.: Contact Mechanics. Springer, Berlin (2018)

Demirhan, N., Kanber, B.: Stress and displacement distributions on cylindrical roller bearing rings using FEM. Mech. Based Des. Struct. Mach. **36**(1), 86–102 (2008)

Deng, S., Hua, L., Han, X., Huang, S.: Finite element analysis of fatigue life for deep groove ball bearing. Proc. Inst. Mech. Eng. Part L J. Mater. Des. Appl. **227**(1), 70–81 (2013)

Deng, B., Guo, Y., Zhang, A., Tang, S.: Finite element analysis of thrust angle contact ball slewing bearing. In: IOP Conference Series: Materials Science and Engineering, vol. 274, p. 012096. IOP Publishing (2017)

Fang, N., Pugh, D., Themudo, R.: On the stress concentration factors of rolling element bearing cages. Tribol. Trans. **50**(4), 445–452 (2007)

Guo, Y., Parker, R.G.: Stiffness matrix calculation of rolling element bearings using a finite element/contact mechanics model. Mech. Mach. Theory **51**, 32–45 (2012)

Hagiu, G., Gafitanu, M.: Dynamic characteristics of high speed angular contact ball bearings. Wear **211**(1), 22–29 (1997)

Hamrock, B.J., Anderson, W.J.: Rolling-element bearings. Technical Report (1983)

He, D., Yang, Y., Xu, H., Ma, H., Zhao, X.: Dynamic analysis of rolling bearings with roller spalling defects based on explicit finite element method and experiment. J. Nonlinear Math. Phys. **29**(2), 219–243 (2022)

Holm-Hansen, B.T., Gao, R.X.: Vibration analysis of a sensor-integrated ball bearing. J. Vib. Acoust. **122**(4), 384–392 (2000)

Jedrzejewski, J., Kwasny, W.: Modelling of angular contact ball bearings and axial displacements for high-speed spindles. CIRP Ann. **59**(1), 377–382 (2010)

Kim, W., Lee, C., Hwang, Y.: A study on the shrink fits and internal clearance variation for ball bearing of machine tool using FEM. In: Proceedings of the International Multi-conference of Engineers and Computer Scientists (2009)

Liao, N.T., Lin, J.F.: Ball bearing skidding under radial and axial loads. Mech. Mach. Theory **37**(1), 91–113 (2002)

Liu, J., Tang, C., Wu, H., Xu, Z., Wang, L.: An analytical calculation method of the load distribution and stiffness of an angular contact ball bearing. Mech. Mach. Theory **142**, 103597 (2019)

Lostado, R., Escribano García, R., Fernandez Martinez, R.: Optimization of operating conditions for a double-row tapered roller bearing. Int. J. Mech. Mater. Des. **12**, 353–373 (2016)

Lovell, M., Khonsari, M.: On the frictional characteristics of ball bearings coated with solid lubricants. J. Tribol. **121**, 761–767 (1999)

Marino, L., Cicirello, A.: Experimental investigation of a single-degree-of-freedom system with Coulomb friction. Nonlinear Dyn. **99**(3), 1781–1799 (2020)

Nazir, M.H., Khan, Z.A., Saeed, A.: Experimental analysis and modelling of c-crack propagation in silicon nitride ball bearing element under rolling contact fatigue. Tribol. Int. **126**, 386–401 (2018)

Schwack, F., Prigge, F., Poll, G.: Finite element simulation and experimental analysis of false brinelling and fretting corrosion. Tribol. Int. **126**, 352–362 (2018)

Shin, G.H., Hur, J.W.: A new finite element analysis model to estimate contact stress in ball screw. Appl. Sci. **12**(9), 4713 (2022)

Singh, S., Köpke, U.G., Howard, C.Q., Petersen, D.: Analyses of contact forces and vibration response for a defective rolling element bearing using an explicit dynamics finite element model. J. Sound Vib. **333**(21), 5356–5377 (2014)

Turek, P., Skoczyński, W., Stembalski, M.: Development of fem model of an angular contact ball bearing with its experimental verification. J. Mach. Eng. **19**(4), 58–69 (2019)

Wang, H., Han, Q., Zhou, D.: Nonlinear dynamic modeling of rotor system supported by angular contact ball bearings. Mech. Syst. Signal Process. **85**, 16–40 (2017)

Xi, H., Lin, T.R., Wang, F., Zhou, Y., Wang, G., Liu, P.: Contact probabilities of an angular ball bearing under a combined axial and radial load. Mech. Mach. Theory **157**, 104196 (2021)

Yongqi, Z., Qingchang, T., Kuo, Z., Jiangang, L.: Analysis of stress and strain of the rolling bearing by FEA method. Phys. Procedia **24**, 19–24 (2012)

Zhang, J., Fang, B., Zhu, Y., Hong, J.: A comparative study and stiffness analysis of angular contact ball bearings under different preload mechanisms. Mech. Mach. Theory **115**, 1–17 (2017)

Zhaoping, T., Jianping, S.: The contact analysis for deep groove ball bearing based on ANSYS. Procedia Eng. **23**, 423–428 (2011)

Publisher's Note Springer Nature remains neutral with regard to jurisdictional claims in published maps and institutional affiliations.